Lawrence Berkeley National Laboratory

LBL Publications

Title

Resilient cooling through geothermal district energy system

Permalink

https://escholarship.org/uc/item/7wp321gf

Authors

Gautier, Antoine

Wetter, Michael

Sulzer, Matthias

Publication Date

2022-11-01

DOI

10.1016/j.apenergy.2022.119880

Peer reviewed

eScholarship.org Powered by the California Digital Library
University of California

Applied Energy 325 (2022) 119880

Contents lists available at ScienceDirect

Applied Energy

journal homepage: www.elsevier.com/locate/apenergy

Resilient cooling through geothermal district energy system

Antoine Gautier [a], Michael Wetter [b,*], Matthias Sulzer [b,c]

[a] Solamen SAS, Beaupreau-en-Mauges, France
[b] Lawrence Berkeley National Laboratory, Berkeley, CA, USA
[c] Empa, Dübendorf, Switzerland

GRAPHICAL ABSTRACT

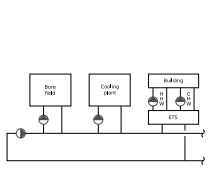

District energy system.

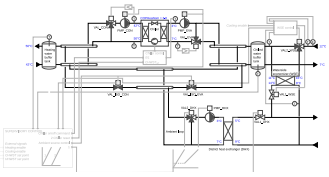

Energy transfer station with heat recovery chiller and optional waterside economizer. Blue indicates design temperatures.

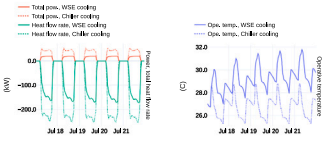

Resulting power consumption, cooling heat flow rate and operative room temperatures in the worst of the 15 thermal zones during the heat wave.
See paper for sensitivity analysis.

Configuration	Resilience week				Whole year		
	P_{max} (kW)	$P_{Chiller}$ (kW)	Q_{max} (kW)	COP (-)	COP (-)	COP_{Sys} (-)	T_{bor} (C)
(a) 700 boreholes, cooling towers downstream, without WSE	1279	1033	5372	4.3	3.9	5.9	[9.0, 21.3]
(b) 930 boreholes, central chillers, with WSE	501	435	4101	8.1	4.2	6.0	[10.5, 15.8]
(c1) 1200 boreholes, cooling towers upstream, with WSE	500	429	4228	8.5	4.4	5.9	[9.4, 15.6]
(c2) 1450 boreholes, cooling towers downstream, with WSE	500	427	4271	8.6	4.4	5.8	[9.1, 15.1]

Performance indices for different district energy configurations and bore field sizes.

ARTICLE INFO

Keywords:
Resilience
District heating and cooling
Geothermal Borefield
Modelica
Modeling and simulation
Numerical performance

ABSTRACT

Decarbonization and resilience to heat waves have recently become high priorities for building and district energy systems. Geothermal coupled district heating and cooling systems that operate a water loop near ground temperature gain increasing adoption to support decarbonization. In these systems, vapor-compression machines, distributed in the energy transfer stations, lift the temperature up or down to the needs of the particular building. In principle, these systems can provide low-power, free cooling from the geothermal bore field during heat waves when electricity is often scarce.

However, the performance of such a resilience operation mode and its implication on the energy system configuration and the sizing of the bore field and HVAC equipment is not yet understood. Consequently, we are assessing their resilience, power use and design implications under a scenario of a heat wave on five working days during which chillers are switched off to reduce electrical consumption. Our analysis is based on high-fidelity, coupled dynamic models of district energy, building-side HVAC and actual control logic, with whole building energy simulation used to assess thermal conditions in a 2004 vintage multi-zone office building in Chicago, IL.

The results show that relying only on waterside economizer cooling, the indoor thermal conditions can be maintained in a tolerable range for the majority of the building zones with half the electrical energy compared to standard chiller operation. Thermal comfort in the hottest zones can be further improved by oversizing the cooling coil. However, the waterside economizer has significant implications on the system configuration and sizing: The geothermal bore field needs to be sized about 30% larger than the upper limit of the range observed for conventional geothermal systems. Nevertheless, if a central chiller plant is added,

* Corresponding author.
E-mail addresses: agautier@solamen.fr (A. Gautier), mwetter@lbl.gov (M. Wetter), matthias.sulzer@empa.ch, msulzer@lbl.gov (M. Sulzer).

https://doi.org/10.1016/j.apenergy.2022.119880
Received 27 April 2022; Received in revised form 1 August 2022; Accepted 17 August 2022
Available online 7 September 2022
0306-2619/Published by Elsevier Ltd. This is an open access article under the CC BY license (http://creativecommons.org/licenses/by/4.0/).

the bore field can be downsized to the typical design range. The latter configuration still allows compressor-less cooling during the heat wave with peak power reduced by 60% compared to the standard design and chiller operation.

1. Introduction

Defined as prolonged periods of excessive heat [1], heat waves are a specific type of extreme temperature event that is regarded by the US National Weather Service as the major cause of weather-related fatalities in the United States [2]. By analyzing regional data sets since the mid-twentieth century, Perkins-Kirkpatrick and Lewis [1] show that the increasing trends of historical heat wave frequency, duration and cumulative intensity have accelerated in many regions over the globe. Futures trends are described by Meehl and Tebaldi [3] who demonstrate that heat waves in Europe and North America will become more intense, more frequent, and longer lasting in the second half of the 21st century. This is in agreement with the conclusions from [4] which states that the surface temperature is projected to rise over the 21st century under all assessed emission scenarios, and that it is very likely that heat waves will occur more often and last longer. As for the consequences of the exposure to heat waves, the report mentions a declining work productivity, an increasing morbidity and mortality. Basu and Samet [5] mention the lack of air conditioning as the first risk factor beside preexisting diseases. This is corroborated by Medina-Ramón and Schwartz [6] who observed the largest effects of heat on mortality in cities with milder summers, less air conditioning and higher population density.

This is especially concerning as heat waves are also well-identified stressors for the electrical grid. Not only are the thermal loads higher during a heat wave, but also the efficiency of most cooling systems drops as the ambient air temperature rises (e.g., between 2% and 3% per Kelvin for air-cooled chillers as a simple Carnot efficiency analysis shows) which tends to further increase the loads on the grid. In addition, the performance of power plants is itself reduced at high ambient temperatures, such as the output capacity and efficiency of gas-fired combustion turbines [7]. This can remove the reserve margins of the grid, which are typically of 15% [8] whereas Ke et al. [7] show an average decrease in the reserve margins of 22% between normal summer days and heat wave days. Burillo et al. [9] thus estimate that power outages could occur up to 30 times more often due to overcurrent tripping, and the probability of cascading failures could increase 30 times as well.

Facing those trends, their impact on human productivity, health and life, and the effects of heat waves on the electricity demand and available capacity of the grid, there is a need to develop innovative cooling systems that can be operated with a low power input at high ambient temperature, so as to rely on a minimum backup capacity during outages and to limit the stress on the grid under normal operation.

In this respect, the so-called combined heating and cooling systems for cold networks appear among the most promising technologies.[1] In addition to providing high efficiency cooling they offer the opportunity to decarbonize heating, which makes them more prevalent in recent development projects. Buffa et al. [10] show an established trend in Europe with about 40 systems in operation as of 2018, and [13] inventories 16 systems in France as of 2020. The specific design we are interested in uses distributed heat recovery chillers that are connected to the main network in which water is circulated near ground temperature, typically between 9 °C and 16 °C. A large central geothermal bore field is used for seasonal heat storage while an optional central cooling plant caters for the annual load imbalance when the heat rejection dominates. The potential benefits of such a design are numerous. The compressor lift is optimized on both sides. On the load side, the supply temperature is driven by the reset logic of each building HVAC system, as opposed to the limiting set point among all connected buildings in case of a central plant. On the source side, the seasonal heat storage yields a higher temperature level at peak heating and a cooler temperature level at peak cooling, and ultimately a chiller efficiency that is largely decorrelated from the ambient temperature. Furthermore, if the heat dissipated at the condenser exceeds the concomitant heating demand in one building, it is rejected into the main loop and contributes to increasing the loop temperature level, which is beneficial to heating dominated buildings. In addition, the low temperature in the main district network enables heat recovery from sources of low-quality heat, such as condenser water from process cooling or even sewage water as low as 15 °C [14]. The low temperature also allows radiant cooling without use of a chiller, or even some comfort cooling as this article will demonstrate. Additionally, uninsulated pipes made of polymeric materials can be used, reducing first costs [10] and potentially increasing the heat storage capacity through the thermal coupling with the ground.

However, those benefits come with some drawbacks. Since the energy transfer stations (ETS) integrate vapor-compression engines, their design and operation is more complex than in the case of simple heat exchangers or even direct connections. Robust hydronic and control principles are paramount when designing the distribution system since any sustained flow imbalance not only results in unmet loads but may lead to chillers tripping out of high condenser pressure. In this respect, Wetter and Hu [14] show that some network topologies are less favorable than others, and can exhibit fast interactions between control loops, yielding pressure imbalances and unstable flow rate. For this reason, and for the better scalability that they provide, unidirectional flow systems appear as the preferred option in this study, although they theoretically exhibit a lower exergy efficiency than bidirectional systems [15] as the exergy is destroyed by mixing, either in the supply pipe in the case of reservoir networks [12], or in the return pipe in the specific design analyzed here. Further, relying on distributed chillers implies a low temperature difference between supply and return in the main loop. Such systems thus require a higher mass flow rate and increased pipe diameters and inevitably lead to a higher pump electricity consumption [10]. Eventually, large geothermal bore fields are expensive to install, especially when the site limitations require deep boreholes [16]. They also make the design and operation more complex due to the required length and resolution of the time horizon [17].

Several articles investigate the efficiency of such systems in configurations where the aggregated load profile is heating dominated and cooling is provided either at low temperature with distributed chillers [14] or at high temperature with intermediary heat exchangers [12], or in cooling dominated configurations for which a central chiller plant is available to provide auxiliary cooling [18]. However, no article could be found that explores the compressor-less cooling potential—which is often presented as a distinguishing feature though—in cooling dominated load profiles—which are the most common cases in mixed-use developments or campus applications. In this

[1] Although the terminology of fifth generation DHC is widely used to refer to those systems [10], it is disputed in [11] which advocates for a distinction in terms of configuration rather than generation, the configuration being called "combined heating and cooling for use in cold networks", the generation remaining the fourth. Referring to a specific hydronic arrangement for that kind of system, Sommer et al. [12] introduce the concept of "reservoir network", which makes explicit another distinguishing feature, that is the low-temperature source that these networks allow connecting to—such as waste heat from process applications, or environmental heat from geothermal plants, or groundwater and lakes. A similar terminology is used in France where the concept of "ambient loop based on geothermal energy" is used [13].

respect, Schluck et al. [15] mentions the lack of detailed models to describe the interplay of the low temperature networks and the consumers' temperatures, especially in the conceptual design process.

This work contributes to bridging this gap. We present a district system for combined heating and cooling that both increases resilience during heat waves and offers a solution to decarbonize heating. In order to propose a generic solution suitable for retrofit, we consider a district with mixed-use buildings equipped with HVAC systems that are representative of existing US buildings, namely all-air systems. We provide a system-level analysis based on dynamic simulations to investigate both the design features—in terms of equipment type, hydronic layout, controls and sizing—and the performance aspects—in terms of power use and indoor comfort during a heat wave, and in terms of annual energy use under standard operating conditions. Because in distributed architectures the ETS is one of the key components of the system, we present the design and operating principles of the ETS and contribute insight on a compressor-less cooling mode that is not addressed in other articles that discuss design challenges. Regarding the seasonal energy storage, we illustrate to what extent conventional sizing methods used for ground-source heat pump systems [19] can inform the design of a large-scale, hybrid and distributed system. We show where those methods fall short, and where a model-based analysis in the time domain becomes necessary for equipment selection and sizing. Eventually we propose design variants that help reduce the size of the bore field which is critical for minimizing first costs.

The paper is organized as follows: In Section 2, an overview of the DHC system is provided as well as a presentation of the computational experiments and the main assumptions used to develop a resilience scenario. This section also includes a brief description of the modeling approach while additional details regarding the modeling principles and challenges are available in Appendix. Section 3 describes the main components of the DHC system, focusing on the equipment characteristics, sizing and operating principles. Section 4 analyzes the performance and resilience of the system when operated either in a low power mode during a heat wave period or under standard conditions over a typical year. The main results are presented and discussed in this section. Concluding remarks are given in Section 5.

2. Description of the simulation experiment

2.1. Overview of the DHC system

Fig. 1 shows the hydronic configuration of the considered DHC system and identifies the modeling approach for each component. The geothermal bore field and the cooling plant are hydronically decoupled from the main network and are equipped with circulation pumps. As described later in the article the cooling plant may be integrated either upstream or downstream of the bore field as represented on the schematic. An ETS is considered at the interface between each building and the main network. Each component of the DHC system is described in detail in Section 3 while the modeling approach is presented in Section 2.2.

2.2. Modeling approach

All the numerical models used in this analysis are developed in the Modelica language [20], with the exception of the building envelope and load model that uses EnergyPlus [21]. The majority of the models are distributed with the Modelica Buildings Library (MBL, see "Data Availability Statement" for the data availability), an open-source library that is based on the Modelica IBPSA Library [22] developed in IBPSA Project 1 [23]. The use of that modeling approach can be readily motivated when enumerating the variables of interest for our analysis, namely the chiller, pump and fan power, that all depend strongly on the control logic such as resetting the chilled water (CHW) supply temperature or the duct static pressure based on actuators' position, or modulating the pump speed based on a differential pressure measurement. Two built-in features of the MBL are critical for that kind of system analysis: the ability to model controls in a physically realistic and efficient way [24], and the pressure-driven fluid flow modeling [25].

In addition, for indoor comfort analysis, we need access to a building room model which enables computing both the air and the indoor surface temperature, which can be coupled to a detailed HVAC system model, and which can be easily parameterized. The MBL comes with the Spawn of EnergyPlus components [26] that implement an automatic co-simulation between Modelica and EnergyPlus. This facilitates the modeling task by providing access to a large stock of prototypical building models and standard load profiles already available for EnergyPlus. Fig. 1 illustrates where the Spawn of EnergyPlus coupling is used.

Table 1
Total conditioned floor area.

Building type	Multiplier factor (-)	Total area (m^2)
Hospital	1	22,422
Medium office	10	49,820
Mid-rise apartment	10	31,340
All buildings	–	103,590

2.3. Building models

We used the commercial reference buildings models [27, 2012] that represent new constructions from 2004 of a medium office, a mid-rise apartment, and a hospital in Chicago IL, USA. Our analysis focuses on the office building type for which resilience metrics are computed based on proxy variables for thermal comfort. The other building types are included to model the load diversity of a typical mixed-use development project. A multiplier factor of 10 is applied to the office and apartment types to represent a cluster of similar buildings. The total conditioned floor area is presented in Table 1.

The building models are used in two different ways. First, simulating those models with EnergyPlus provides heating and cooling loads which are used to size the systems. The domestic hot water (DHW) loads are not considered in this study because they only marginally contribute to the overall demand side energy (see Fig. 2) and because disregarding them results in a conservative assessment of the ground temperature, with a reduced heat removal. Fig. 2 shows the resulting loads integrated over the year. The total peak cooling and heating loads are 6.8 and 5.3 MW (65 and 50 W/m^2), respectively, and the annual energy is 8.9 and 5.8 GWh/a (86 and 56 $kWh/(m^2 \cdot a)$). For the apartment and hospital, the corresponding time series are then directly used as inputs to the DHC system model. The boundary conditions of the Modelica DHC system model at the load side of the ETS component are the building loads, which are converted into a mass flow rate and temperature variation with an interface component that approximates the emission characteristic of the building HVAC system using idealized fan coil models.

Second, for the office type, the EnergyPlus input data file is used directly by the Modelica model, which automatically couples EnergyPlus for a co-simulation using the Spawn of EnergyPlus integration [26]. The Modelica model includes the building HVAC system, the controls, as well as the air volume of the rooms, and the building envelope is simulated in EnergyPlus. Modelica synchronizes the two domains

[2] The DHW loads computed with EnergyPlus for the hospital correspond to only 2% of the end use energy which seems unreasonably low for that building type. Bawaneh et al. [28] rather show that water heating amounts to more than 10% and up to 30% of the end use energy for healthcare facilities in the United States. This discrepancy is further disregarded in our analysis that is focused on space heating and cooling loads.

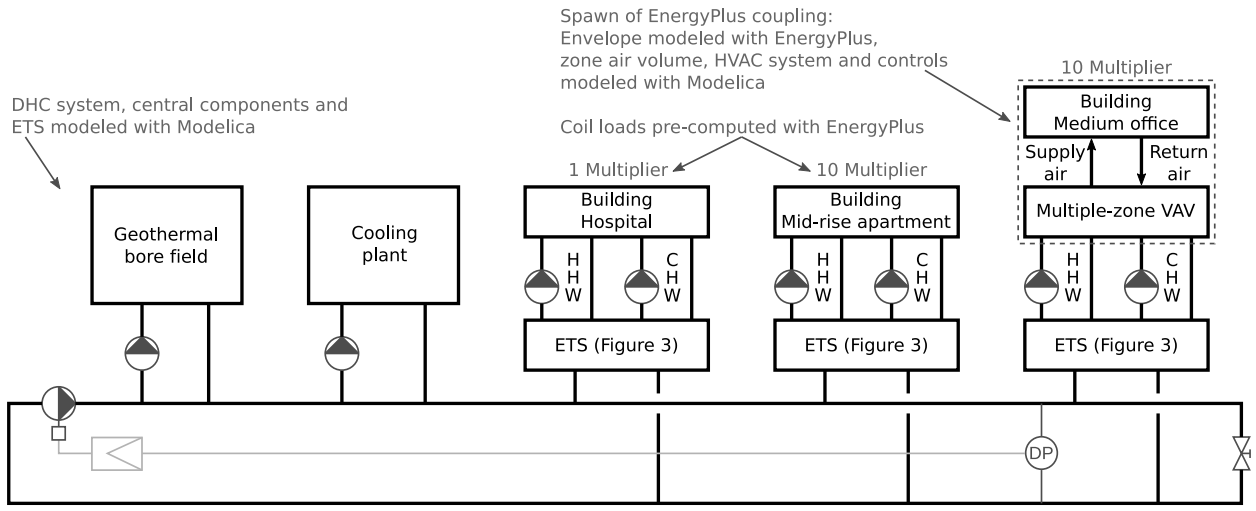

Fig. 1. Schematic diagram of the DHC system. The energy transfer stations (ETS) are served by a two-pipe distribution system where the pump speed is modulated to track a remote pressure differential (DP) set point. Each ETS produces chilled water (CHW) and heating hot water (HHW) distributed to the building HVAC system. A variable air volume system (VAV) is modeled for the office building while an idealized terminal unit model is considered for the other building types. Pipes and ducts are represented with black lines, electrical connections with gray lines, whereas the modeling approach is described in gray font.

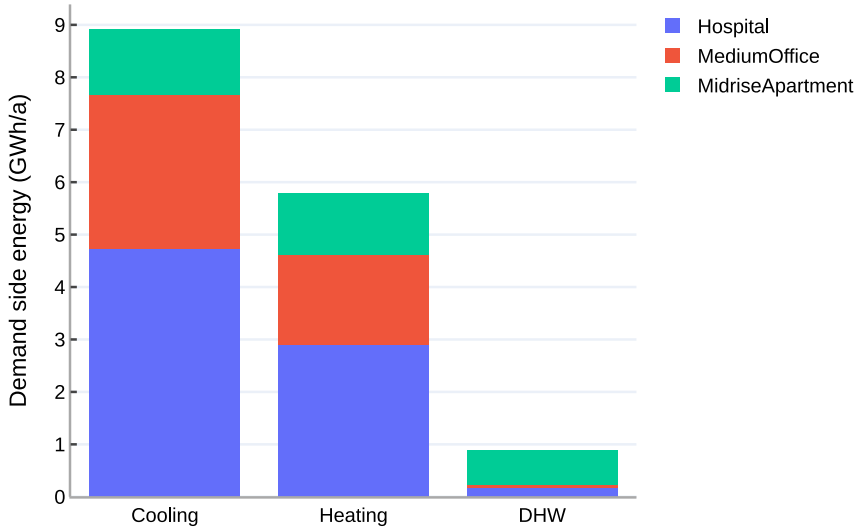

Fig. 2. Building loads computed with EnergyPlus, integrated over the year, including the multiplier factors used to represent clusters of similar buildings. (DHW loads are presented for reference but are not considered in this study.[2])

by exchanging temperature and heat flow rates. The building HVAC system is a variable air volume (VAV) system with hot water reheat. The system components are sized based on the peak loads computed with EnergyPlus (with a cooling load diversity factor of 0.7) and the requirements from [29] for ventilation parameters. The cooling coil leaving air temperature is 13 °C at design conditions, which yields a design air flow rate of $44,478\,\mathrm{m^3/h}$, and an air change rate between 3 and $9\,\mathrm{h^{-1}}$ among the conditioned zones. The control sequence is adapted from [30]. The main features of the control implementation are described in [31], and were adapted for our model which contains 15 conditioned zones plus 3 plenum zones for the air return.

2.4. Resilience scenario and metrics

To analyze the resilience of the DHC system, we used weather data and internal heat gains as follows:

We used hourly weather data for annual simulation, from a typical meteorological year (TMY3) for Chicago, IL, USA. However, we modified the file to include a so-called "resilience design day", which we generated based on the most severe conditions in July from that TMY3 weather file.[3] During the resilience design day the dry-bulb temperature range is [23.3, 35] °C, the wet-bulb temperature range is [22.5, 26.9] °C, and the global horizontal irradiance peaks at $931\,\mathrm{W/m^2}$. The resilience design day is repeated to create 5 consecutive days in July that represent a five-day office week with a heat wave over which the comfort analysis is performed.

We adapted the nominal heat gains from the original EnergyPlus input data file to account for a reduced occupancy scenario during the resilience week where the office building operates on backup power.[4] The nominal number of people and plug power is reduced by 30% and the nominal lighting power is reduced by 70%.

[3] These conditions are more severe than a design day generated based on the method proposed in [32] Chapter 14 considering the annual 0.4% design dry-bulb temperature of 33.3 °C and the mean coincident wet-bulb temperature of 23.7 °C.

[4] This assumption differs from [33] where only the loss of the HVAC system is considered without any concomitant reduction in the internal heat gains.

The key metrics and the methodology to evaluate the resilience of the office building during the resilience week are taken from [33]. The number of degree-hours beyond a tolerable limit of 30 °C is computed for each thermal zone.[5] Mathew et al. [33] consider that the zone cannot be occupied if that number exceeds 34 K · h per day while the temperature is still beyond tolerable. This contributes to increasing a so-called number of occupant hours lost (OHL) by the number of people that would otherwise be present in the zone. To support the analysis of cases where the number of OHL is zero for all thermal zones, we also compute the number of degree-hours above the tolerable limit of 30 °C. In addition, we only count for degree-hours during typical operating hours from 7am to 7pm, from Monday to Friday.

3. Description of the main components of the DHC system

We will now describe the main components of the DHC system, including the sizing and control approach because system-level performance is sensitive to the proper sizing and control of the individual components.

3.1. Energy transfer station

Fig. 3 shows the schematic diagram of the ETS and the design conditions that were used for sizing its components. A similar ETS concept was first investigated for a mixed-use development project with distributed geothermal bore fields in [14]. It relies on heat recovery chillers,[6] and a load balancing control logic that uses the ambient source—the service water through the interface heat exchanger—to reject excess heat or excess cold depending on the actual operating conditions.

We will now summarize the main operating principles. For further details, we refer to the documentation of the model `Experimental.DHC.EnergyTransferStations.Combined.Generation5.ChillerBorefield` distributed within the Modelica Buildings Library (commit 4a6285f).

- The supervisory controller ensures that the load is balanced between the condenser side and the evaporator side of the chiller. Heating (resp. cooling) is enabled based on an external demand signal from the building automation system (see Section 3.2). When enabled, the mode remains active for at least 15 min and, when disabled, the mode cannot be enabled again for at least 15 min.
  The temperature at the top of the heating hot water (HHW) buffer tank is controlled within a dead band above the supply temperature set point. When heating is enabled, a PI controller is activated and tracks the lower limit of the dead band. The controller yields a cold rejection signal $u_{Rej,Col}$ which is used to create a false load on the evaporator (see the district heat exchanger control hereunder) and thus increase the heat transfer rate at the condenser. Another PI controller tracks the upper limit of the dead band and yields a heat rejection signal $u_{Rej,Hea}$. This second controller is activated when there is no cold rejection demand, which is detected based on the closed end switch contact of the evaporator isolation valve `VAL_ISO_EVA`.
  The maximum signal between heat and cold rejection $u_{Rej} = \max(u_{Rej,Col}, u_{Rej,Hea})$ is used to control in sequence the district heat exchanger, and then the chiller, by resetting down the CHW supply temperature. The CHW supply temperature reset is performed within a range bounded by the minimum evaporator leaving temperature from the chiller specification at the lower end, and the minimum between the CHW supply temperature set point from the building automation system (see Section 3.2) and the service water entering temperature minus 3 K at the higher end. The latter limit avoids operating the ambient loop at maximum flow rate when the CHW supply temperature set point from the building automation system is higher than the service water entering temperature—which typically occurs in the heating season with low cooling demand and low district water temperature.
  In addition, when cooling is enabled, a PI controller tracks the CHW supply temperature set point at the bottom of the CHW buffer tank. This controller limits the cold rejection when the set point is not met. This is needed because of the parallel arrangement of the evaporator loop and the ambient loop, where the latter can "steal" primary flow rate that will not reach the buffer tank, which can lead to secondary flow recirculation and increasing the temperature at the bottom of the tank. This will create a demand that will limit the flow rate in the ambient loop. Note that secondary flow recirculation may still happen if the chiller set point (as set by the supervisory controller) is lower than the CHW supply temperature set point (as set by the building automation system).
  This control logic based on opposing PI controllers was preferred to a discrete logic based on a set of operating modes, where short cycling between the different modes was difficult to avoid.
  The only remaining discrete control logic pertains to the actuation of the isolation valves `VAL_ISO_CON` and `VAL_ISO_EVA` between the condenser and evaporator loops and the ambient loop. Here a simple logic based on the return position of the opposite valve and a non zero heat or cold rejection demand, $u_{Rej,Hea}$ or $u_{Rej,Col}$, is implemented to open the valve. Timers are used to avoid short cycling.
- The district heat exchanger (DHX) hydraulically decouples the building system and the district system. It is controlled using the heat or cold rejection signal u_{Rej} from the supervisory controller as an input. The primary and secondary circuits are enabled to operate if u_{Rej} is greater than zero and at least one isolation valve `VAL_ISO_CON` or `VAL_ISO_EVA` is proven open. When enabled, the secondary circuit is controlled based on u_{Rej}, which is mapped to modulate in sequence the mixing valve `VAL2_DHX` and the pump speed of the pump `PMP_DHX`. (The mixing valve is needed to stabilize the control of the system when the secondary mass flow rate required to meet the heat or cold rejection demand is below the minimum flow rate to operate the pump.) The opening of the primary valve `VAL1_DHX` is directly modulated with u_{Rej}.
  This was preferred to a control based on the temperature levels on each side of the heat exchanger due to the variation of the temperature difference between the secondary and primary side when switching between heat rejection (with large temperature difference) and cold rejection (with small temperature difference, as used for sizing). This required gain scheduling and turned out to be difficult to tune. However, the simpler logic based on the heat or cold rejection demand brings additional requirements regarding hydronic balancing, see Appendix.
- The waterside economizer (WSE) is enabled if there is a cooling demand, and the evaporator isolation valve is closed (i.e., the system is not in cold rejection mode, otherwise the excess cold should be used first to cool the building), and the predicted leaving water temperature at the WSE is lower than the entering water temperature. Timers are used to avoid short cycling. The

[5] For simplicity we use the operative temperature, as opposed to the standard effective temperature in [33].

[6] Heat recovery chillers are typically built with scroll or screw compressors that are capable of operating with condenser water leaving temperature as high as 60 °C [34]. That makes the equipment suitable for both heating hot water and domestic hot water production. The drawback is that the compressor is operated at a high lift which is detrimental to the efficiency. A potentially more efficient design is proposed in [35] where at least two separate units are used and the source-side circuits are connected together with the ambient source (a geothermal bore field in that case), resulting in cascading thermodynamic cycles when the plant operates in simultaneous heating and cooling mode.

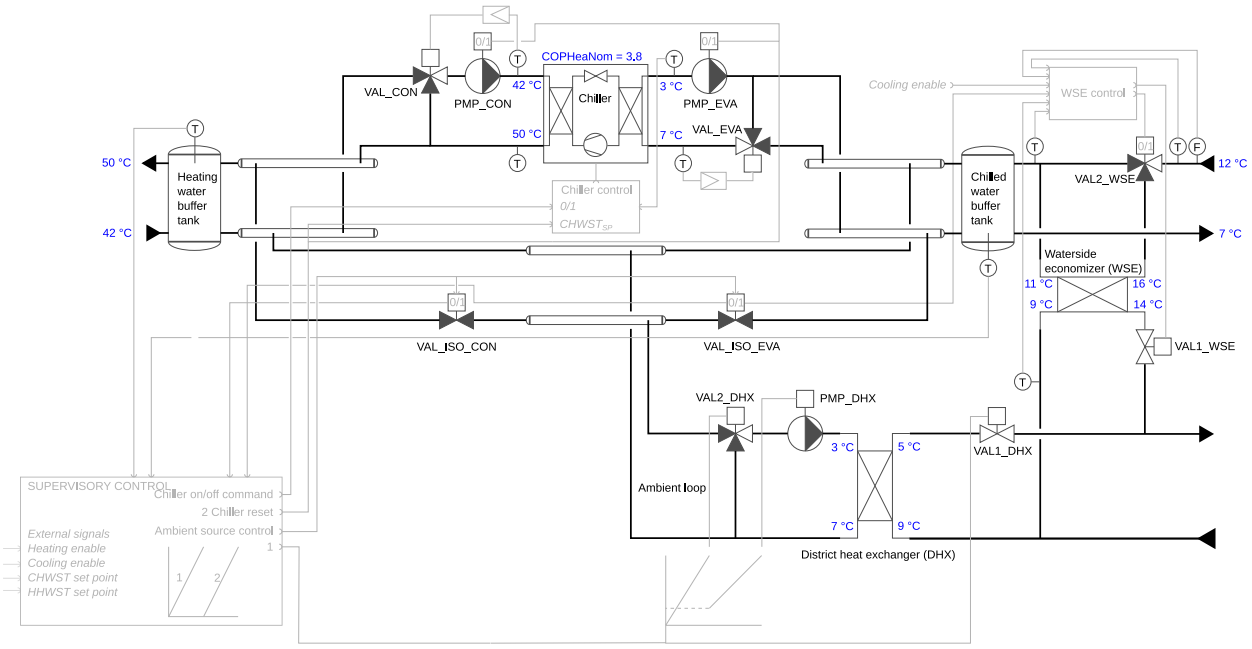

Fig. 3. Schematic diagram of the energy transfer station used in this study. Pipes are represented with thick black lines, electrical connections with thin gray lines, whereas the blue font indicates the design values.

system is disabled if any of the above conditions is not met, except that the actual leaving water temperature is used instead of the predicted one. When the system is enabled, the bypass valve `VAL2_WSE` on the secondary side of the WSE is fully closed and the opening of the primary valve `VAL1_WSE` is modulated so that the primary flow rate varies linearly with the secondary flow rate.
The WSE is integrated sidestream where the CHW temperature is the warmest to maximize the rate of heat transfer at given mass flow rates. However, it is not integrated into the condenser loop but rather connected to the district loop. This means that a dedicated heat exchanger is used, distinct from the district heat exchanger. The reason is that the WSE is intended to be operated not only in a resilience mode instead of the chillers, but also in conjunction with the chillers during the shoulder or cold season with a low service water temperature and low cooling loads that allow resetting the CHW supply temperature. Under those conditions, it is likely that simultaneous heating loads require a high condenser temperature that is higher than the CHW return temperature. The WSE is sized with a 2 K approach and the design values of the CHW mass flow rate and temperature difference. This differs from the design in conventional chilled water plants where the WSE is sized at partial load. The objective here is to reach the maximum cooling capacity in the resilience mode during a heat wave.

- The condenser and evaporator pumps `PMP_CON` and `PMP_EVA` are enabled when heating or cooling is enabled and when the CHW tank requests to be charged. The latter condition is required to avoid operating the pumps and the chiller when the cooling load is already met by the WSE. When enabled, the pumps are operated at constant speed, and the condenser (resp. evaporator) mixing valve `VAL_CON` (resp. `VAL_EVA`) is modulated with a PI loop controlling the minimum (resp. maximum) inlet temperature. The chiller is enabled when the pumps are proven on. It is controlled based on the CHW supply temperature set point yielded by the supervisory controller.

3.2. Demand signal, supply temperature reset and secondary pump control

We describe here the control sequence for the in-building distribution systems and the reset strategy based on terminal unit demand signals.

The heating and cooling demand signals are computed based on the maximum control signals of the terminal units: whenever a terminal controller yields a non-zero signal (implemented using a small hysteresis) the demand signal switches to true.

If there is no demand, the secondary pump is disabled, and the supply temperature is reset to the least extreme value, allowing the chiller to operate at low lift.

If there is a demand, the secondary pump is enabled and its speed is modulated with a PI controller to track a differential pressure set point at the most remote unit,[7] and the supply temperature is reset with a PI controller that tracks the maximum opening of the control valves of the terminal units to match 90%. We noticed that it is important to reset the controller output so that the design set point value is used when the demand signal switches to true. Otherwise there is a significant delay in satisfying the load, followed by a large overshoot, and the control loop is hard to tune.

3.3. Central systems

3.3.1. Loop temperature range

The supply temperature in the main loop is allowed to float between 9 °C and 16 °C to satisfy the constraints on

- the minimum temperature of the fluid leaving the evaporator, which is typically around 3 °C for water without glycol, and the CHW ΔT, which is set at 4 K for the primary circuit,

[7] Modern control sequences [36] use a cascade control and reset in sequence the differential pressure set point of the distribution pump (up, first) and the CHW supply temperature set point (down, last) when the number of requests yielded by the terminal units increases—giving the priority to maintaining a low compressor lift over a low pump speed—although such sequenced control is shown to be only slightly better than resetting the CHW supply temperature alone.

- the maximum CHW supply temperature in WSE-only mode, which is set at 18 °C—a typical value for radiant cooling systems which is considered here as the maximum value to provide comfort cooling with all-air systems, and
- the heat exchanger approach, which is taken equal to 2 K at design conditions for both the district heat exchanger and the WSE.

The lower limit of that range is reduced to 5 °C outside of the heating season when the constraint on the minimum temperature of the fluid leaving the evaporator is no more limiting. A sensitivity to the upper limit of that range is provided in Section 4.1 to give more ground to the retained assumption.

3.3.2. Hydronic network

We modeled uninsulated HDPE pipes, with a hydraulic diameter computed based on a design pressure drop of 100 Pa/m. A trench length of 200 m is considered between each building, as well as a 50 m long service line.

The main distribution pump is sized considering a load diversity factor of 0.9 as observed on the load data (see Section 2.3). The speed of the main distribution pump is modulated with a PI controller that tracks a constant pressure differential set point at the boundaries of the most remote ETS. A bypass line is modeled and is sized to recirculate 5% of the design flow rate at the pressure differential set point.

3.3.3. Geothermal bore field

In this paragraph we describe the main characteristics of the ground heat exchanger while providing a first assessment of the number of boreholes based on a conventional sizing method, for both the heating and cooling requirements. The simulation study will then explore the sizing range in-between those two numbers. The main question we answer is to what extent the size of the bore field can be reduced—adopting a hybrid system design that uses dynamic simulations—while still providing enough capacity to maintain the loop supply temperature under 16°C during an extreme week.

Kavanaugh and Rafferty [19] propose a sizing method for bore fields that are used for heating and cooling. Their method recommends a total borehole length L (m) of

$$L = \frac{\dot{Q}_y R_y + \dot{Q}_m R_m + \dot{Q}_h \left(R_b + F_{sc} R_h\right)}{\left(T_{Ent} + T_{Lvg}\right)/2 - \left(T_g + T_p\right)}, \tag{1}$$

where $\dot{Q}_y$, $\dot{Q}_m$ and $\dot{Q}_h$ are the net average heat flow rates transferred to the ground on a yearly, monthly and 6-hour basis, respectively (counted positively for heat rejection to the ground[8]), R_y, R_m and R_h are the effective thermal resistances of the ground computed with a 10-year, 1-month and 6-hour heat pulse, respectively, R_b is the borehole overall thermal resistance, $F_{sc} = 0.04$ is a correction factor for short-circuit heat losses between the upward and downward flowing legs, T_g is the undisturbed temperature of the ground, T_p is the ground temperature penalty that takes into account long-term effect of annual load imbalance, T_{Ent} is the temperature of the liquid entering the probes, and T_{Lvg} is the temperature of the liquid leaving the probes.

The effective resistance of the ground is computed according to the cylindrical heat source formulation from [37] considering a borehole diameter of 150 mm, a soil conductivity, specific heat capacity, and density of 2.3 W/(m · K), 1000 J/(kg · K), and 2600 kg/m^3, respectively. This gives $R_y = 0.17\,\text{m} \cdot \text{K/W}$, $R_m = 0.15\,\text{m} \cdot \text{K/W}$, and $R_h = 0.08\,\text{m} \cdot \text{K/W}$. The overall resistance of the borehole is computed based on the method from [19] considering DN40 DR11 HDPE pipes in a double-U configuration and a grout material with a conductivity of 2.0 W/(m·K), which gives $R_b = 0.06$ m · K/W. The hourly load data are generated as described in Section 2.3. They are used to compute the heat flow rate transferred to the main network (see Fig. 4) based on a chiller coefficient of performance of

$$COP_{Cooling} = \frac{\dot{Q}_{Evaporator}}{P} = 7.0,$$

in cooling mode. This COP is based on a condenser entering temperature of 18 °C and an evaporator leaving temperature of 7 °C, which yields a high COP due to the low compressor lift at peak cooling load. For heating, the coefficient of performance is

$$COP_{Heating} = \frac{\dot{Q}_{Condenser}}{P} = 4.0,$$

which is based on an evaporator entering temperature of 7 °C and a condenser leaving temperature of 50 °C. Those values are representative of a modern high-efficiency screw compressor unit with a cooling capacity in the order of 1 MW.[9] They are chosen at the cooling and heating design conditions, respectively. The reason is that the 6-hour and monthly contributions largely prevail in Eq. (1) (see for instance Fig. 6 for an illustration of the respective contributions).

The sizing rationale is then as follows: Starting from an undisturbed ground temperature of $T_g = 10$ °C, the load profile dominated by heat rejection will enable reaching an equilibrium temperature of $T_g + T_p = 12$ °C, which lies roughly in the middle of the target loop temperature range of $[9, 16]$ °C. From there, the cooling plant balances the heat transferred to the main loop on an annual basis, so $\dot{Q}_y = 0$ W is considered to size the bore field. The effect of the cooling plant on $\dot{Q}_m$ and $\dot{Q}_h$, i.e., near cooling design conditions, is neglected as explained in Section 3.3.4. With a borehole depth of 180 m, this gives $n_{Heating} = 705$ boreholes for heating and $n_{Cooling} = 1426$ boreholes for cooling. Now considering $T_g + T_p = 11$ °C instead of 12 °C would give a required number of $n_{Heating} = 881$ boreholes for heating and $n_{Cooling} = 1224$ boreholes for cooling. The preliminary sizing is therefore highly sensitive to the unknown temperature penalty T_p. Its value depends on several factors that are simple assumptions at that stage of the design, such as the capacity of the cooling plant to balance the load profile over the year, the seasonal performance of the ETS chillers, and the characteristics of the bore field (number and length of the boreholes, field arrangement and separation distance, soil characteristics). That is mainly what the simulation analysis will further help specifying.

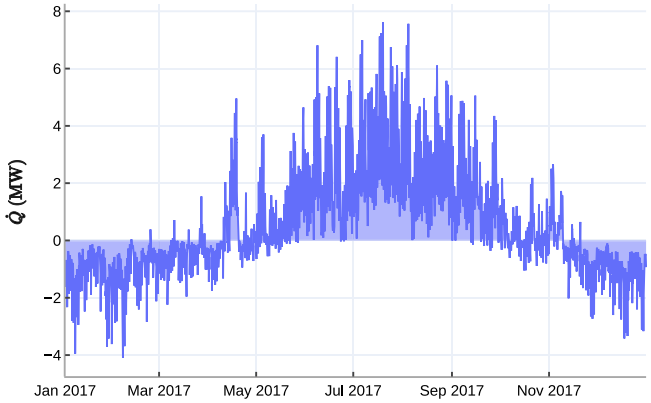

Fig. 4. Hourly heat flow rate transferred to the main network (computed from EnergyPlus load data, see Section 2.3).

3.3.4. Cooling plant

The selection of the cooling system can be informed by the weather data statistics, shown in Fig. 5, and the contribution of the different heat pulses to the sizing of the bore field based on Eq. (1) and shown in

[8] This is the opposite convention as the one used in [19], and Eq. (1) is rearranged accordingly.

[9] The chiller performance data used in the simulation model (see $COP_{Heating} = 3.8$ in Fig. 3) are consistent with those values.

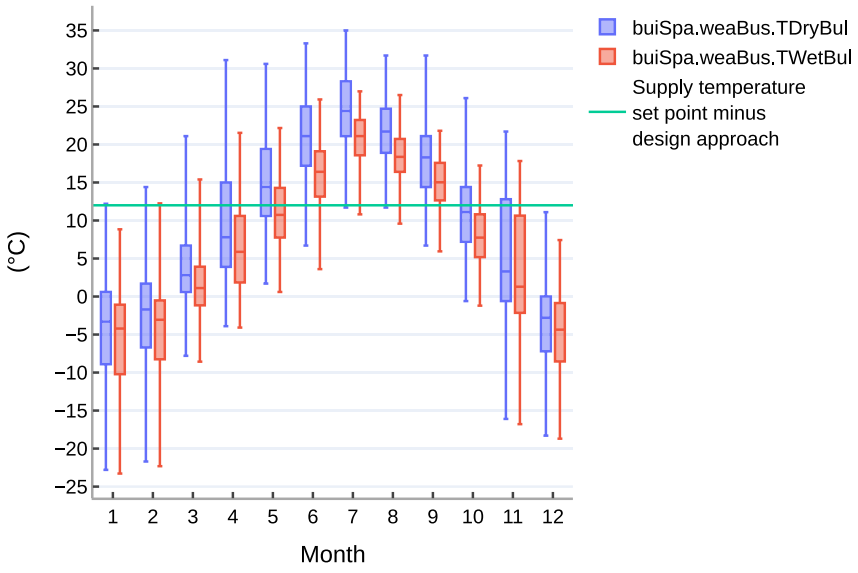

Fig. 5. Monthly box plots of the hourly dry-bulb and wet-bulb temperature from the typical meteorological year (TMY3) for Chicago, IL. The whiskers show the minimum and maximum values, the boxes show the first, second—median—and third quartiles.

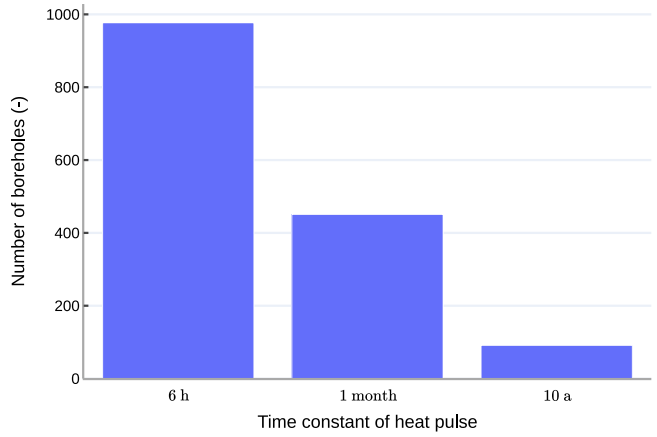

Fig. 6. Contribution of the different heat pulses to the sizing of the bore field based on Eq. (1) (including the yearly average not considered if compensated by a cooling plant).

Fig. 6. If open cooling towers or dry coolers are used,[10] they will mainly be off during the hottest months as the maximum allowed loop supply temperature is 16 °C. The cooling system will be primarily used during the shoulder seasons to cool down the bore field, and to balance the heat transferred to the main loop on an annual basis. Considering the annual component in Fig. 6, the impact of the annual load on the size of the bore field is only about 10%. Therefore, if the supply temperature must be kept under 16 °C to allow WSE cooling, the highest number of boreholes $n_{Cooling}$ is likely required. This will be verified by modeling an open cooling tower plant with an intermediary heat exchanger. As the plant is designed to balance the heat transferred to the main loop on an annual basis, a whole-year simulation of the coupled system is needed for a proper sizing.

The control sequence of the plant is as follows: The system is enabled based on a similar logic as the one implemented for the WSE, see Section 3.1: The controlled variable is the minimum water temperature in the main loop downstream of the connection to the plant. A predicted value of that controlled variable is computed and the system is enabled if it is at least 1 K lower than the temperature in the main loop upstream of the connection to the plant. When enabled, a cascade control is used: The first controller tracks the controlled variable. The output signal of that controller first increases the speed of the heat exchanger pumps, and then resets the water temperature at the outlet of the towers. A second controller tracks the water temperature at the outlet of the towers and is used to modulate the fan speed. The system is disabled if the actual value of the controlled variable is higher than the temperature in the main loop upstream of the connection to the plant—which might occur at minimum pump speed, minimum fan speed (or in free convection mode) and high outdoor wet-bulb temperature.

We will also analyze an alternate design that uses central air-cooled chillers to lower the heat rejection demand during the hottest months, and that enables downsizing the bore field. An additional simulation experiment will be carried out to assess to what extent and with what control strategy such a configuration can provide compressor-less cooling during a heat wave, i.e., keep the supply temperature of the loop under 16 °C without enabling the chillers. This configuration can be used together with the previous one so that the cooling towers serve as condenser water coolers, and a waterside economizer mode enables cooling the main loop at low ambient temperature.

4. Results

This section first presents the analysis of the indoor thermal comfort during the resilience week in a compressor-less operating mode. The models only cover the building and HVAC systems, while the water temperature in the supply service line is a fixed boundary condition. The main objective is to assess the margins that a conventional VAV system design offers for comfort cooling when the chilled water temperature exceeds its design value, and the sensitivity of those margins to high-level sizing parameters. In Section 4.2, we discuss the characteristics of the central components of the DHC system that are required to maintain the supply temperature in the acceptable range. Lastly, in Section 4.3 the system performance is analyzed.

[10] Open cooling towers allow approaching the wet-bulb temperature up to 2 to 4 K but require an intermediary heat exchanger to prevent an elevated oxygen concentration in the district loop. They can be operated even at low ambient temperature, under freezing conditions. Dry coolers can economically cool water to within approximately 10 K of the ambient dry-bulb temperature and can be directly connected to the district loop. To avoid the addition of anti-freeze protection, they shall be enabled only if the ambient temperature is above 0 °C.

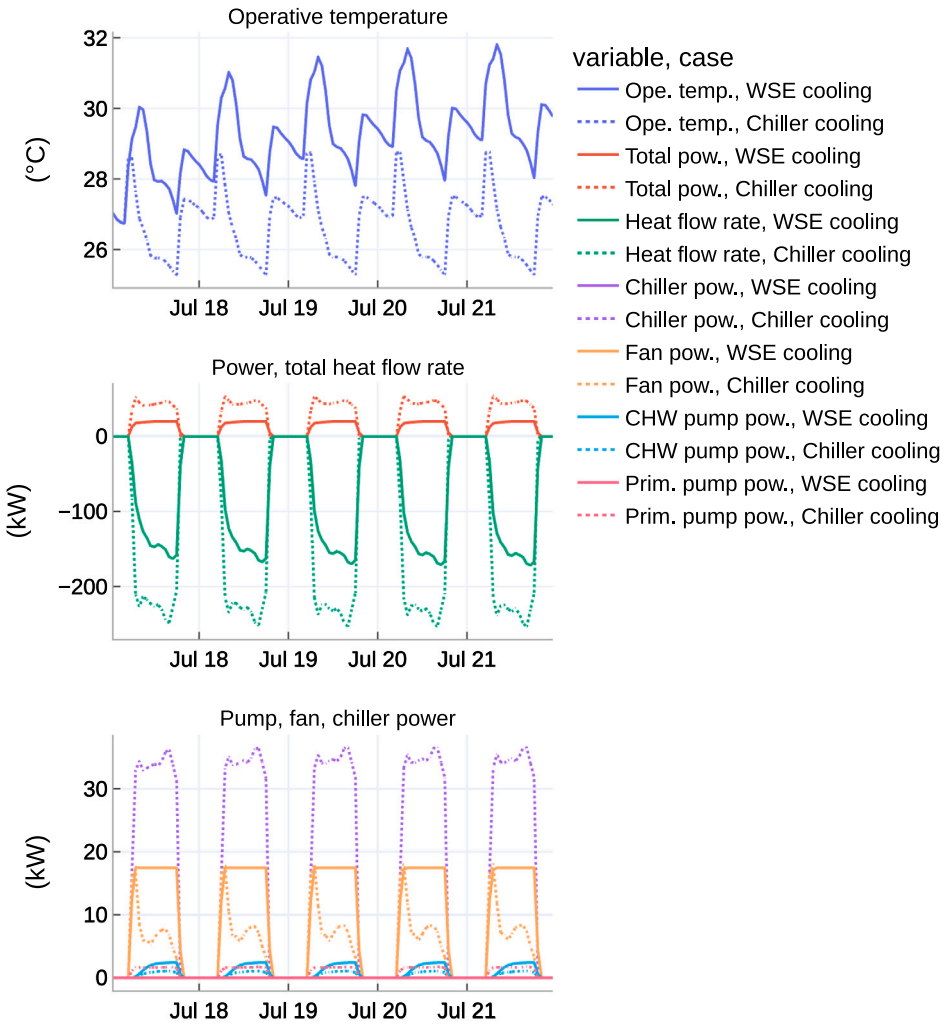

Fig. 7. Operative temperature in the limiting zone (first plot); total power and cooling heat flow rate (second plot); chiller, pump and fan power (third plot). WSE cooling (solid lines) is compared to chiller cooling (dotted lines) during the resilience week.

4.1. Indoor thermal comfort in a compressor-less operating mode

Disabling the chillers, because of power shortage, and relying only on WSE cooling during the resilience week with a water supply temperature of 16 °C in the service line does not yield any OHL in the office building. The evolution of the operative temperature is provided in Fig. 7, together with the power drawn by the fans, pumps and chillers, and the total cooling heat flow rate. The case with WSE-only cooling is compared to the base case with standard chiller operation. The WSE-only mode yields a reduction of about 60% in the total power at the peak, while still meeting 70% of the load. This is achieved despite a high chiller COP close to 7 in the base case. The relative importance of the fan power partly results from the high design air flow rate (between 3 and 9 h^{-1} among the conditioned zones) and emphasizes the challenge that all-air systems represent as opposed to radiant systems. During the operating hours the average building HVAC system COP (accounting for the AHU fan, the primary and secondary pumps, and the chiller) is equal to 5.2 in the base case with standard chiller operation and 7.3 in the case of WSE-only cooling.

The number of degree-hours above the tolerable limit is presented in Fig. 8 for each of the 15 thermal zones in the case with WSE-only cooling. With a water supply temperature of 16 °C in the service line, the number of degree-hours is below 7 K h in the limiting zone during the limiting day, so far below 34 K h per day which is considered in [33] as the limit to decide that a zone cannot be occupied and to start incrementing the thermal OHL count. The median number of degree-hours remains equal to zero, meaning that a tolerable thermal comfort can be achieved in a low-power mode in the majority of the thermal zones.

Loop supply temperature. The sensitivity to the district loop supply temperature is illustrated in Fig. 8. This provides an ex post justification of the choice of the temperature range in Section 3.3.1, as one can observe that the majority of the thermal zones exhibit degree-hours above tolerable during the limiting day for a temperature higher than 16 °C.

Cooling coil sizing. The sensitivity to the cooling coil capacity is analyzed by applying a multiplier factor to the design UA-value of the coil model. We also increased the design pressure drop by the same factor for both the air and the chilled water side. The CHW pump and fan design flow rate is considered identical in all cases. Only the design head is increased to accommodate the higher pressure drop. To some extent, this is compatible with reusing the installed CHW pump or fan, provided that sizing margins are available on the total head at maximum speed, which is typically the case.

As illustrated in Fig. 9, oversizing the coil by a factor of 1.6 reduces the number of degree-hours above the tolerable threshold by 40% for the limiting zone, while the average power during the operating hours is increased by about 20% and the total cooling heat flow rate is increased by about 10%, which leads to a reduction in system

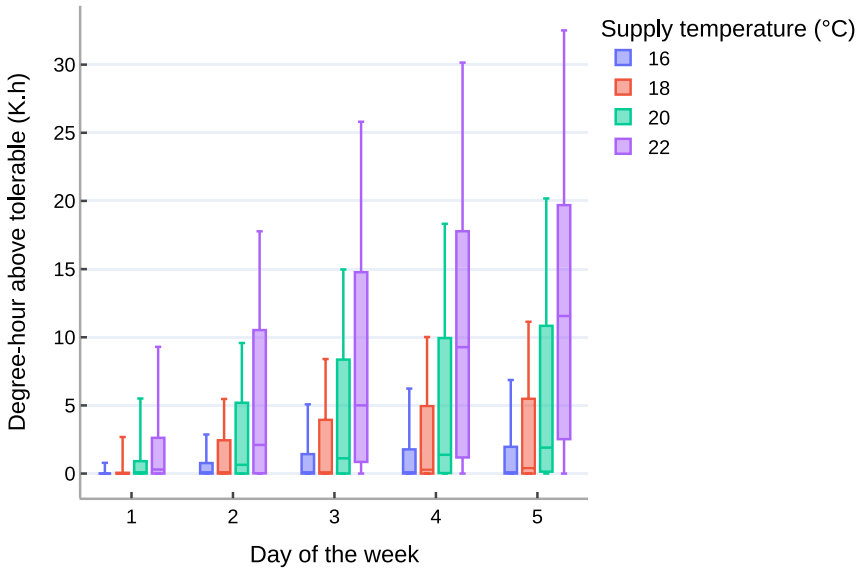

Fig. 8. Daily box plots of degree-hours above tolerable threshold of 30 °C as distributed over all thermal zones. The different colors illustrate the sensitivity to the district loop supply temperature. The whiskers show the minimum and maximum values, the boxes show the first, second—median—and third quartiles.

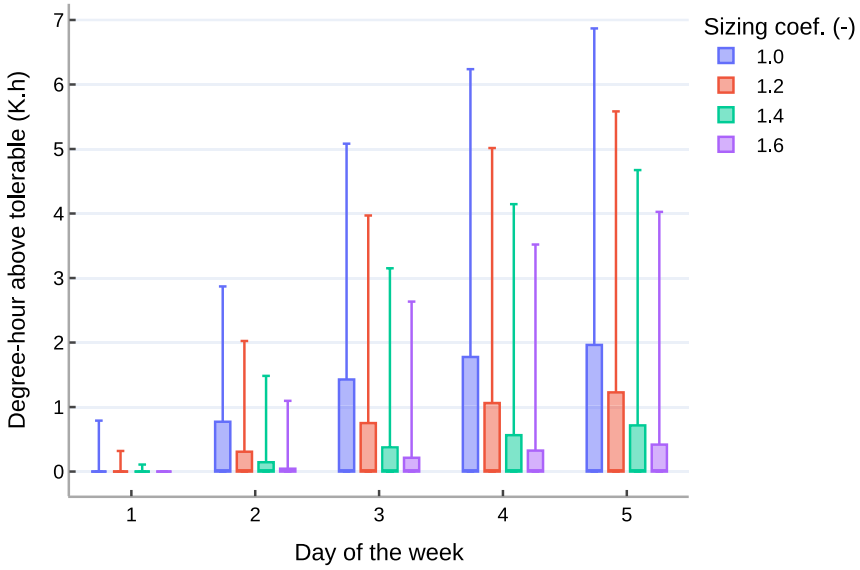

Fig. 9. Daily box plots of degree-hours above tolerable threshold of 30 °C as distributed over all thermal zones. The different colors illustrate the sensitivity to the cooling coil sizing. The whiskers show the minimum and maximum values, the boxes show the first, second—median—and third quartiles.

COP from 7.3 to 6.9. However, it is worth noting that part of the oversizing could be achieved by integrating a change-over valve on the heating coil and connecting it to the CHW distribution system in the compressor-less cooling mode (where the high CHW temperature prevents condensation on the coil). This would limit the increase in the fan power and the reduction of the COP.

Fan sizing. The sensitivity to the fan sizing is analyzed by applying a multiplier factor k to the nominal volume flow rate and k^2 to the nominal head of the fan. The flow resistance of the duct network and all other AHU components is considered identical in all cases. Our premise is that the integration into an existing system can be made by only changing the AHU fan.

As illustrated in Fig. 10, oversizing the fan has a limited impact on the number of degree-hours above the tolerable threshold, with an optimum appearing around 20%. This is because of two reasons: First, the power drawn by the fan motor scales cubic with the sizing factor, and so does the dissipated heat. This leads to an increase in the supply air temperature. Second, with increased flow rate but constant heat exchange area, the effectiveness of a heat exchanger approaches asymptotically a limit. Hence, increasing flow rate has generally a diminishing benefit. Comparing the base case $k = 1$ with the optimum case $k = 1.2$, the average power during the operating hours is increased by about 60% while the total cooling heat flow rate is increased by less than 10%, which corresponds to a reduction in system COP from 7.3 to 4.8. The latter value indicates that the WSE-only cooling mode with an oversized fan is less efficient than the chiller cooling mode.

4.2. DHC central components

Geothermal bore field and cooling towers. Figs. 11 and 12 show the sensitivity to the size of the bore field by plotting the supply temperature and the transferred energy as computed by simulating five years of operation for different numbers of boreholes within the range determined in Section 3.3.3. Fig. 12 shows that the energy transferred

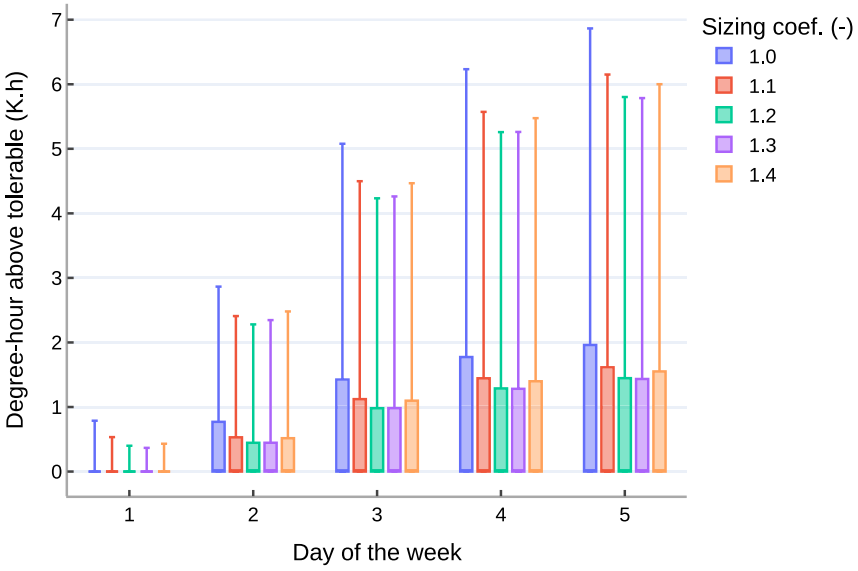

Fig. 10. Daily box plots of degree-hours above tolerable threshold of 30 °C as distributed over all thermal zones. The different colors illustrate the sensitivity to the fan sizing. The whiskers show the minimum and maximum values, the boxes show the first, second—median—and third quartiles.

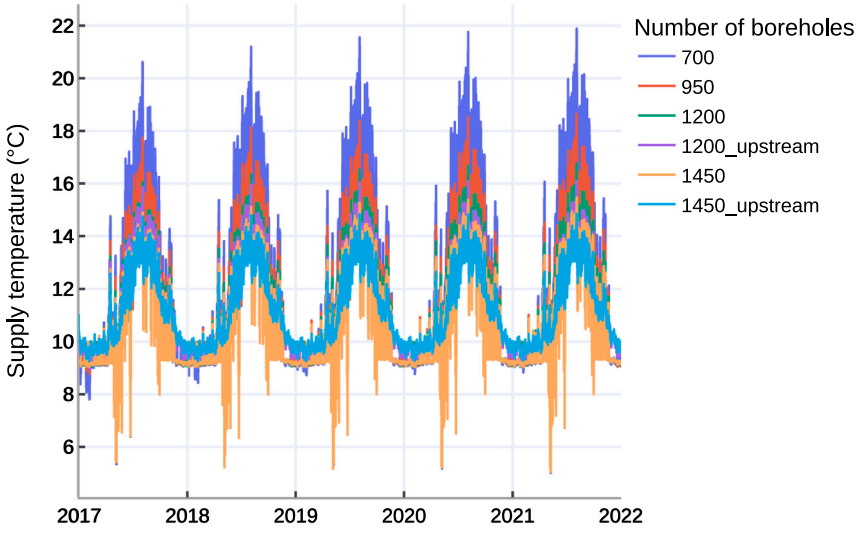

Fig. 11. District water supply temperature in the case with central cooling towers, over five years of operation. The different curve colors illustrate the sensitivity to the geothermal bore field sizing and to the integration of the cooling towers—either downstream of the bore field, or upstream of the bore field if suffixed with *upstream*.

to the ground is flattening out on an annual basis and, hence, the five year horizon can be used to analyze the operation. This verifies that the initial sizing based on Eq. (1) is appropriate for that hybrid system with cooling towers. When the cooling towers are integrated downstream of the bore field, the maximum number of boreholes of 1450 is indeed required to maintain the supply temperature below 16 °C. When the cooling towers are integrated upstream of the bore field, their cooling capacity is increased due to a higher inlet temperature and a lower supply temperature set point. The lower supply temperature set point is possible because of the temperature regained through the bore field, as illustrated in Fig. 13. Due to this increased cooling capacity, a lower average ground temperature can be reached, allowing a reduction in the number of boreholes to 1200. Fig. 13 also illustrates that integrating the cooling towers upstream of the bore field yields a higher supply temperature in the heating season, which will further improve the heating efficiency of the ETS.

Depending on the cooling tower integration, the bore field sizing ratio is between 32 and 38 m/kW (total length of boreholes divided by the system cooling capacity) which lies outside of the range of [10, 25] (m/kW) typically encountered for conventional geothermal systems [19]. This is explained by the low temperature approach of about 6 K (to the undisturbed ground temperature) that is required here for the ground heat exchanger, as opposed to the range of [10, 25] °C generally used for conventional geothermal systems without any requirement for compressor-less cooling. ETH [38] provides another reference for comparison. In this so-called "anergy grid" a cooling capacity of 3 MW at design conditions is provided by a geothermal system composed of 431 boreholes of 200 m length, that is a sizing ratio of 29 m/kW for a maximum temperature of 18 °C in the cold ring. The order of magnitude is consistent with our results if we take into account the different temperature approach that is unfavorable in our case. Nevertheless, such a high sizing ratio for the geothermal system implies a first cost that may be prohibitive for many development projects and calls for exploring a hybrid design with a lower number of boreholes and central chillers, which is the subject of the section below.

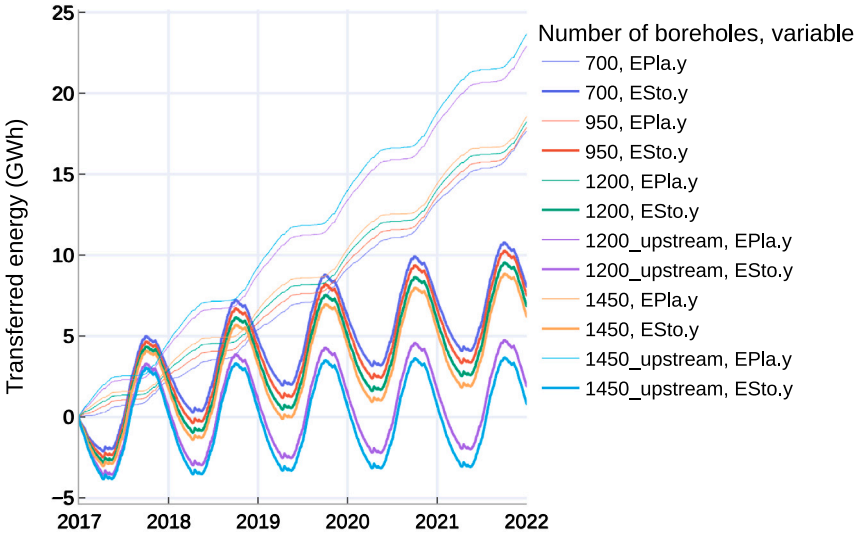

Fig. 12. Energy transferred from the district loop through the bore field $ESto.y$ (thick lines) and through the cooling towers $EPla.y$ (thin lines) in the case with central cooling towers, over five years of operation. The different curve colors illustrate the sensitivity to the geothermal bore field sizing and to the integration of the cooling towers—either downstream of the bore field, or upstream of the bore field if suffixed with *upstream*.

Table 2
During the resilience week operating hours (first group of columns): Total power P_{Max} and cooling heat flow rate $\dot{Q}_{Max}$ at peak load, average value of total power P_{Mean} and coefficient of performance COP for all DHC and HVAC systems. Over a whole year of operation (second group of columns): Average value of coefficient of performance for both heating and cooling, for all DHC and HVAC systems COP and for ETS chillers only COP_{Chi}, and range of district water supply temperature T_{Sup} (heating season only for the minimum, see Section 3.3.1).

Configuration	Resilience week				Whole year		
	P_{Max} (kW)	P_{Mean} (kW)	$\dot{Q}_{Max}$ (kW)	COP (-)	COP (-)	COP_{Chi} (-)	T_{Sup} (°C)
(a) 700 boreholes, cooling towers downstream, without WSE	1279	1033	5372	4.3	3.9	5.9	[9.0, 21.3]
(b) 950 boreholes, central chillers, with WSE	501	435	4101	8.1	4.2	6.0	[10.5, 15.8]
(c1) 1200 boreholes, cooling towers upstream, with WSE	500	429	4228	8.5	4.4	5.9	[9.4, 15.6]
(c2) 1450 boreholes, cooling towers downstream, with WSE	500	427	4271	8.6	4.4	5.8	[9.1, 15.1]

Geothermal bore field and central chiller plant. This section explores the effect of replacing the cooling towers with a chiller plant with air-cooled chillers, and whether doing so allows to reduce the number of boreholes. Using air-cooled chillers gives the supply temperature trajectory shown in Fig. 14 during the fifth year of operation. In this configuration, both the central chillers and the distributed chillers are disabled during the resilience week so that the cooling function only relies on the ground heat exchanger and the WSE. In the first experiments the central plant is controlled to track the maximum loop supply temperature set point of 16 °C. The variants shown in dotted lines use different temperature set points.

When controlling for the maximum loop supply temperature set point, we can observe that the central chillers do not help reduce the number of installed boreholes and that the maximum size of the bore field is still required to keep the temperature below 16 °C during the resilience week. The fact that the supply temperature is higher on an average than in the case with the cooling towers reveals a reduced precooling of the bore field, and calls for modifying the controls to better leverage the cooling capacity of the plant, which we will do next.

As a simple control alternative, the temperature set point of the plant is first reduced to 11 °C in the configuration with the smallest bore field size (700), i.e., the highest temperature approach for the ground heat exchanger. This configuration is close to meeting the temperature requirement during the resilience week, however, it exhibits a sustained temperature drop below the minimum set point during the heating season. This behavior is the consequence of a lower amount of heat stored in the ground over the period where heat rejection dominates—part of it being released into the atmosphere by the central cooling plant. The last configuration tested uses 950 boreholes and a temperature set point of the plant of 12 °C and meets the temperature range requirement. The ground heat exchanger is here sized with about 25 m/kW of total borehole length per cooling capacity, which falls within the upper range of the sizing ratios observed on conventional geothermal systems [19] and below the value of 29 m/kW from the anergy grid in [38]. However, this raises additional questions regarding the optimal control of such a system as the central chillers are mainly operated during the hot season during which their efficiency is lowest. Precooling the ground at maximum chiller efficiency without jeopardizing winter operation would require additional research.

4.3. System performance

The system performance is evaluated on different time horizons and operating conditions: First and foremost over a five day resilience week where the system is operated in a low power mode, then over a whole year under standard operating conditions. For system configurations that include a WSE, the chillers are disabled during the resilience week and cooling is provided by the WSE only. Alternatively, under standard

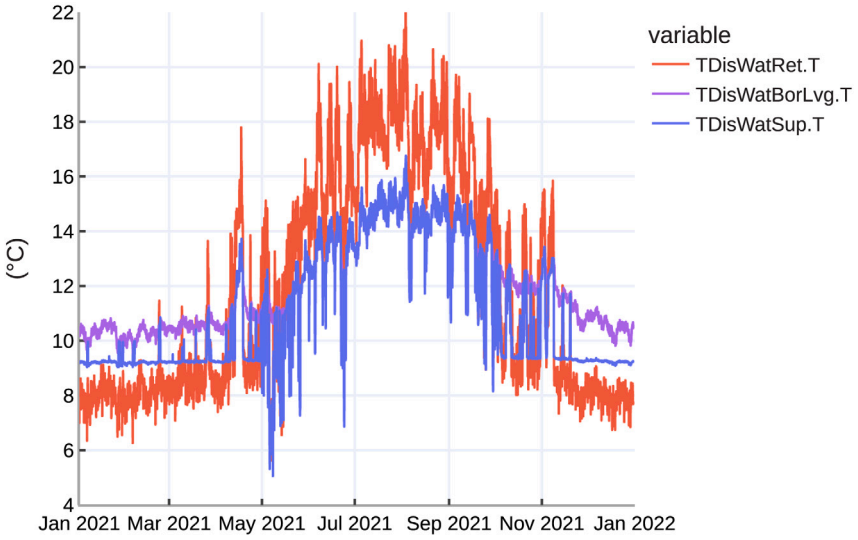

(a) Cooling towers downstream of the bore field.

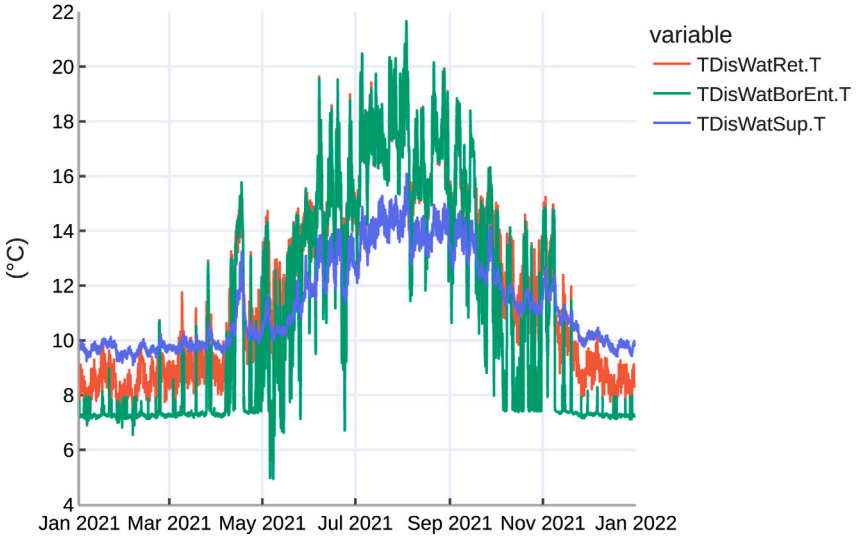

(b) Cooling towers upstream of the bore field.

Fig. 13. District water supply $TDisWatSup.T$ and return temperature $TDisWatRet.T$, bore field entering $TDisWatBorEnt.T$ or leaving temperature $TDisWatBorLvg.T$ in the case with central cooling towers and 1200 boreholes, over the fifth year of operation. Figure (a) represents the configuration with the cooling towers integrated downstream of the bore field. Figure (b) represents the configuration with the cooling towers integrated upstream of the bore field.

operating conditions, both the chillers and the WSE can contribute to the cooling function.

Table 2 provides the peak and mean power drawn by the DHC and HVAC systems, as well as the cooling heat flow rate distributed to the buildings, and the overall coefficient of performance. Four configurations are compared. In configuration (a) no WSE is included, all chillers are operated even during the resilience week, the central plant consists of cooling towers and the lowest number of boreholes is considered. In configuration (b) a WSE is included, all chillers are disabled during the resilience week, the central plant consists of air-cooled chillers and the optimum number of boreholes is considered. In configurations (c1) and (c2) a WSE is included, all chillers are disabled during the resilience week, the central plant consists of cooling towers and the optimum number of boreholes is considered. Configurations (c1) and (c2) differ by the integration of the cooling towers either upstream of the bore field (c1) or downstream of the bore field (c2). Fig. 15 provides the electricity consumption breakout for the three configurations (a), (b) and (c1).

The first assessment from Section 4.1 can be updated by considering now the whole impact of the WSE mode, including the impact on the operating point of the district distribution pump and the actual loop temperature. The WSE mode yields a reduction of more than 60% of the peak power during the resilience week, whereas it still enables meeting about 80% of the load. This holds true for all the configurations with WSE, so either with a large bore field and cooling towers, or with a lower number of boreholes and a central chiller plant. This translates into an overall coefficient of performance that is about twice higher than in configuration (a) with standard chiller operation during the

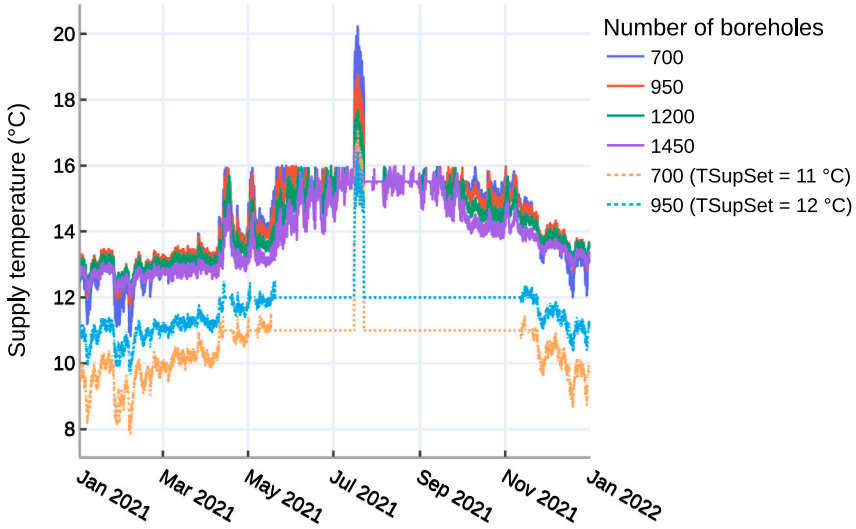

Fig. 14. District water supply temperature in the case with central chillers, over the fifth year of operation. The different curve colors illustrate the sensitivity to the geothermal bore field sizing and to the supply temperature set point (highlighted by dotted lines).

resilience week. The fact that the COP is higher than the one that was first assessed in Section 4.1 when considering only the ETS and the HVAC systems of the office building is due to the lower fan power to cooling capacity ratio for the other building types where idealized fan coil models are used. In that case the ratio falls around 0.05 W/W whereas it is close to 0.1 W/W for the office building for which a detailed model of a VAV system is implemented with the Spawn of EnergyPlus co-simulation.

Comparing those results with the monitored performance of the anergy grid over a whole year of operation [38] is daunting at first as the latter exhibits seasonal COP values between 22.1 and 36.5 for compressor-less cooling (including pumping energy). However, those values do not factor in the input power of the building HVAC systems. Excluding the fan power in our case yields a COP value of 23.9 for the configuration (c1) during the resilience week where the district water temperature is the highest, so where the pumping energy to the cooling output is also at its maximum. Once again the impact of the fan power (already illustrated in Fig. 7) reveals the challenge of providing cooling at low power in the case of all-air systems.

Regarding the annual performance, the three configurations with WSE are close to one another and the most favorable one (c1) yields only 13% gain on the seasonal COP for heating and cooling compared to the configuration without WSE (a). This is mainly because the building air systems are not favorable to the use of high CHW temperature and limit the contribution of the WSE mode during standard operation (e.g., to 12% of the total cooling energy for the office building).

The comparison with the monitored performance of the anergy grid [38] is limited to the only cluster of that system that includes active cooling by means of heat pumps. The average value of the coefficient of performance of the heat pumps for both heating and cooling over 10 months of operation amounts to 6.9, which is to be compared with the value of COP_{Chi} between 5.8 and 6.0 in our case. Considering the favorable temperature levels at which both the CHW (12 °C or 18 °C as opposed to 7 °C at design conditions in our case) and the HHW (34 °C as opposed to 50 °C at design conditions in our case) are produced in the anergy grid provides a first explanation for that 15% performance gap. Another reason may be found in the possible loss of exergy efficiency due the unidirectional flow in our case, as opposed to the bidirectional flow with cold and hot rings in the case of the anergy grid. Although recent comparisons between bidirectional and unidirectional designs show little impact on the total electricity consumption [12], they only cover configurations with compressor-less cooling. The effect of a cold loop on the chiller efficiency and on the occurrence of WSE cooling could favor bidirectional systems for the kind of applications studied here.

Among other possible factors that could enhance the system performance, the type of HVAC systems certainly comes first. Integrating radiant cooling systems in the buildings would benefit all configurations as it allows lowering the chiller lift, and it would favor even more the configurations with WSE by increasing the numbers of WSE operating hours. The size of the geothermal bore field would also be reduced by the reduced amount of heat rejected to the main loop. In addition, for cooling dominated applications like the one being presented here, having dedicated chillers for heating and cooling with cascading thermodynamic cycles (see for instance [35]) would benefit, in particular, the configurations with WSE which operate the district loop at a lower temperature. With heat recovery chillers as in our experiments, during times of simultaneous heating and cooling loads, the favorable loop temperature does not translate into a gain on the chiller lift because the chiller must be operated at a high condenser temperature compatible to serve the heating load, as opposed to the minimum temperature allowing heat rejection to the district system.

5. Conclusion

Ambient loop DHC systems are considered to be one of the most efficient technologies to harvest waste heat at a large scale. However, the fact that mixed-use developments often exhibit a yearly load profile dominated by heat rejection, together with the trend in the cooling demand of urban systems, motivate the investigation of the cooling efficiency of such systems, and the compressor-less cooling potential that is often designated as one of their core characteristics. The large geothermal bore fields that are often integrated into those systems especially contribute to the acceptance that they are indeed perfect candidates for low power cooling operation.

In our experiments, we used all-air systems to provide space cooling as these are most common in US commercial buildings. However, these systems are also least favorable for compressor-less cooling. Using a system design approach guided by numerical simulation, we conclude that the requirements for compressor-less cooling put significant constraints on the equipment selection and sizing. In our experiments, it turns out that only about 10% of the total cooling energy can be provided with compressor-less cooling. Moreover, the low temperatures required for cooling in all-air systems leads to large bore fields, which raises the question of the economic viability, notably if the option of a central chiller plant is ruled out. For resilient design, and also for energy

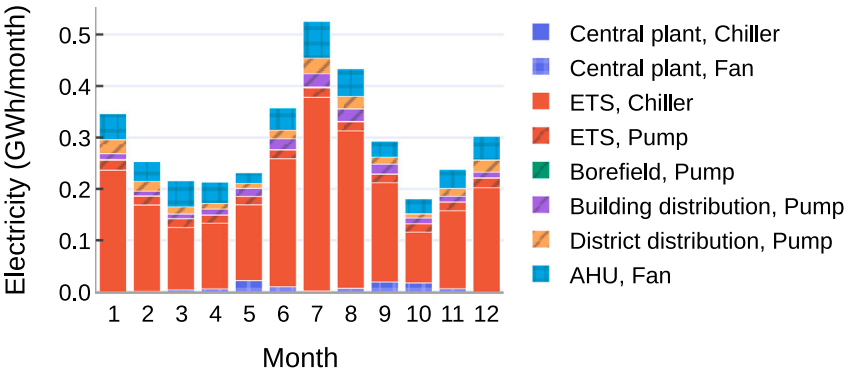

Configuration (a) 700 boreholes, cooling towers downstream, without WSE.

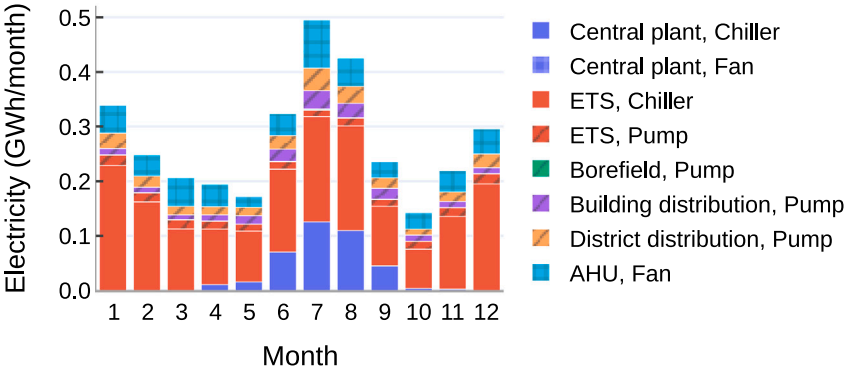

Configuration (b) 950 boreholes, central chillers, with WSE.

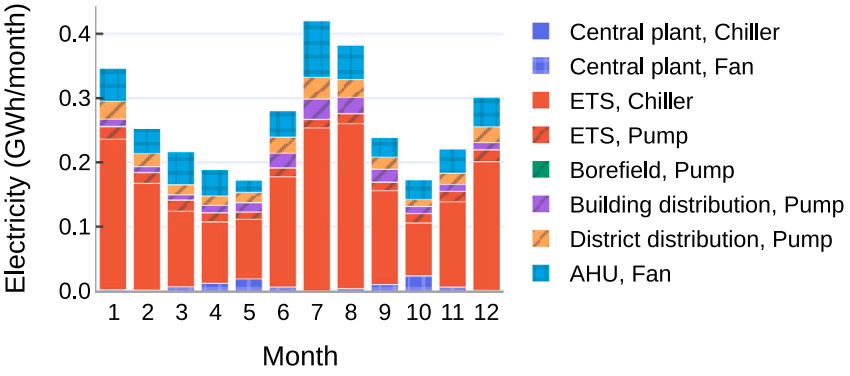

Configuration (c1) 1200 boreholes, cooling towers upstream, with WSE.

Fig. 15. Monthly electricity consumption over a typical year of operation. The three figures correspond to different system configurations.

efficiency, system-level optimization is therefore critically important: If radiant cooling systems were used, such as chilled ceilings, the number of compressor-less operating hours would rise substantially, and the bore field could likely be downsized.

For the examined all-air systems, disabling the chillers and solely relying on geothermal cooling through a WSE during a hot resilience week where electricity consumption may have to be reduced, our results show that the total power drawn (from central DHC systems to HVAC terminal units) is reduced by more than 60%, while 80% of the load can still be met, maintaining the indoor thermal conditions in a tolerable range for the majority of the building zones. Hence a resilient urban energy infrastructure can certainly benefit from such design, and even more so if the building systems are also optimized for high temperature cooling, which would further increase the thermal comfort during a heat wave and power shortage. Moreover, high-temperature cooling devices would both alleviate the sizing constraints on the geothermal system and increase the seasonal efficiency of the system.

CRediT authorship contribution statement

Antoine Gautier: Conceptualization, Methodology, Software, Validation, Formal analysis, Investigation, Data curation, Writing – original draft, Writing – review & editing, Visualization. **Michael Wetter:** Conceptualization, Methodology, Software, Validation, Formal analysis, Investigation, Data curation, Writing – review & editing, Supervision, Project administration, Funding acquisition. **Matthias Sulzer:** Conceptualization, Methodology, Validation, Investigation, Writing – review & editing, Supervision.

Declaration of competing interest

The authors declare the following financial interests/personal relationships which may be considered as potential competing interests: Michael Weter reports financial support was provided by US Department of Energy. Mathias Suller reports financial support was provided by Empa Materials Science and Technology. Abntoine Gauter reports financial support was provided by US Department of Energy.

Data availability

All data are available from https://github.com/lbl-srg/ldrd-resilient-district-design commit 021420f that depends on MBL version 8.x development, commit d06ded5.

Acknowledgments

This work was supported by the Laboratory Directed Research and Development Program of Lawrence Berkeley National Laboratory under U.S. Department of Energy Contract No. DE-AC02-05CH11231. Most of the component models that this work relies on were developed in projects supported by the Advanced Manufacturing Office and the Building Technologies Office of the U.S. Department of Energy, under the same contract number.

Appendix. Modeling hydronic systems

When integrating the ETS model into the whole DHC system model, significant effects of hydronic imbalance were first observed, with the remote ETSs being starved and unable to meet the supply temperature set point, and the ETSs closer to the pump operating at higher flow rates than design. In addition, convergence issues of the Newton solver appeared, mainly related to the waterside economizer operation.

The first effect was certainly expected using a pressure-driven model of the hydronic system, with no specific care for balancing the connected units. However, and as in real systems, that effect was not expected to disturb the operation to the extent that was observed. Indeed, a controller that controls for instance the supply temperature or a temperature difference, should limit the primary flow rate to its design value, provided that the primary fluid temperature remains close to the design value. In addition, the heat emission characteristic limits the impact of flow shortage, with 50% of the design mass flow rate still providing about 90% of the design heat flow rate for a heat exchanger with 10 K primary temperature range at design. The only disturbing effects that were expected, and indeed observed, pertain to the low valve authority of the primary control valves that causes control issues, and to the pump speed which is often maxed-out due to the inability to maintain the pressure drop at the remote ETS.

The reason why the ETSs close to the pump often operate at a higher flow rate than design is related to the control based on the heat or cold rejection demand (see Section 3.1) that first opens the primary control valve (up to its full opening), then resets down the CHW supply temperature. So the ETSs that are exposed to a higher differential pressure than the design value use the excess flow rate instead of resetting down the CHW supply temperature and increasing the temperature difference between each side of the heat exchanger.

Regarding the numerical issues that were encountered we acknowledge the challenges that remain when modeling closed loop hydronic systems (typically with feedback of a remote differential pressure sensor or of the valve positions to control the main distribution pump). There has been extensive work that was already carried out to formulate actuator models limiting the size of the DAE systems and exhibiting the proper smoothness required by Newton solvers [39]. Namely, each actuator model of the MBL offers the option to solve either for the mass flow rate or for the pressure drop, which breaks the algebraic loop created when two actuators are in parallel or in series, respectively. In addition they provide the option for an additional state variable (mimicking the actuator motion delay) which is another means to avoid an algebraic loop. In our case, those two modeling features did not solve the convergence issues.

The resolution came from integrating a pressure independent control valve (PICV) into the ETS model to modulate the mass flow rate of the service water through the heat exchangers. To represent the various technologies of PICVs (dynamic balancing valve in series with a control valve, or built-in flow meter and controller) the model `Fluid.Actuators.Valves.TwoWayPressureIndependent` from the MBL idealizes the physics by solving the simple equation $\dot{m}_{Act} = u\,\dot{m}_{Nom}$, where u is the control signal and $\dot{m}_{Act}$ and $\dot{m}_{Nom}$ are the actual and design mass flow rate, respectively. The complexity of the model lies in the requirement to properly represent the valve limiting flow characteristics (leakage and full opening) and to compute a pressure drop and a mass flow rate that are continuously differentiable while transitioning between the two characteristics, which is a requirement of Newton solvers. Using that valve model to modulate the service water flow rate offers key benefits, similar to the ones obtained by the use of PICVs in real hydronic systems. The benefits include:

1. The system is dynamically balanced. The primary flow rate can only marginally exceed the design value. Furthermore, this holds true for any operating point, and any location in the distribution network. To the contrary, balancing valves that are commissioned at design conditions may lead to low pressure differences at the boundaries of the control valves close to the distribution pump in the case of closed loop control based on a remote pressure drop sensor and with low demand on the remote valves.
2. The control is close to linear. The relationship between the control signal (varying between 0 and 1) and the mass flow rate (varying between close to 0 and close to the design value) is indeed close to linear. To the contrary, with standard control valves, a potentially large range of flow rate variation (spanning beyond the design value) may be mapped to a limited range of variation of the control signal (depending on the valve authority), leading to tedious controller tuning or control instabilities.

In addition, the simulation model is simplified due to the ideal model of the flow rate control loop, for instance when modeling a waterside economizer where the primary valve position is actuated so that the primary mass flow rate is equal to the chilled water mass flow rate. This eliminates the need for a controller and the potential need for tuning the control loop, while reducing the number of state variables and therefore the time to solution, especially for such control loops with fast pressure-driven dynamics.

References

[1] Perkins-Kirkpatrick S, Lewis S. Increasing trends in regional heatwaves. Nature Commun 2020;11. http://dx.doi.org/10.1038/s41467-020-16970-7.
[2] Robinson PJ. On the definition of a heat wave. J Appl Meteorol (1988-2005) 2001;40(4):762–75, URL http://www.jstor.org/stable/26184479.
[3] Meehl GA, Tebaldi C. More intense, more frequent, and longer lasting heat waves in the 21st century. Science 2004;305(5686):994–7. http://dx.doi.org/10.1126/science.1098704.

[4] IPCC. Climate change 2014: Synthesis report. Contribution of working groups I, II and III to the fifth assessment report of the Intergovernmental Panel on Climate Change. Technical report, Geneva, Switzerland: IPCC; 2014, p. 151.

[5] Basu R, Samet JM. Relation between elevated ambient temperature and mortality: A review of the epidemiologic evidence. Epidemiol Rev 2002;24(2):190–202. http://dx.doi.org/10.1093/epirev/mxf007.

[6] Medina-Ramón M, Schwartz J. Temperature, temperature extremes, and mortality: A study of acclimatisation and effect modification in 50 US cities. Occup Environ Med 2007;64(12):827–33. http://dx.doi.org/10.1136/oem.2007.033175.

[7] Ke X, Wu D, Rice J, Kintner-Meyer M, Lu N. Quantifying impacts of heat waves on power grid operation. Appl Energy 2016;183:504–12. http://dx.doi.org/10.1016/j.apenergy.2016.08.188.

[8] Burillo D, Chester MV, Ruddell B, Johnson N. Electricity demand planning forecasts should consider climate non-stationarity to maintain reserve margins during heat waves. Appl Energy 2017;206:267–77. http://dx.doi.org/10.1016/j.apenergy.2017.08.141.

[9] Burillo D, Chester M, Ruddell B. Electric grid vulnerabilities to rising air temperatures in arizona. Procedia Eng 2016;145:1346–53. http://dx.doi.org/10.1016/j.proeng.2016.04.173, URL https://www.sciencedirect.com/science/article/pii/S1877705816301801, ICSDEC 2016 – Integrating Data Science, Construction and Sustainability.

[10] Buffa S, Cozzini M, D'Antoni M, Baratieri M, Fedrizzi R. 5th generation district heating and cooling systems: A review of existing cases in Europe. Renew Sustain Energy Rev 2019;104:504–22. http://dx.doi.org/10.1016/j.rser.2018.12.059.

[11] Sulzer M, Werner S, Mennel S, Wetter M. Vocabulary for the fourth generation of district heating and cooling. Smart Energy 2021;1:100003. http://dx.doi.org/10.1016/j.segy.2021.100003.

[12] Sommer T, Sulzer M, Wetter M, Sotnikov A, Mennel S, Stettler C. The reservoir network: A new network topology for district heating and cooling. Energy 2020;199:117418. http://dx.doi.org/10.1016/j.energy.2020.117418.

[13] AFPG. La boucle d'eau tempérée à énergie géothermique. Technical report 01/RGEOTBE01 XM-HL-JMP, Paris, France: AFPG; 2020, URL https://www.geothermies.fr/sites/default/files/inline-files/APFG_GUIDE_BoucleEau_BAT3.pdf.

[14] Wetter M, Hu J. Quayside energy system analysis. Technical report LBNL-2001197, Berkeley, CA: Lawrence Berkeley National Laboratory; 2019, URL https://simulationresearch.lbl.gov/wetter/download/LBNL-2001197.pdf.

[15] Schluck T, Kräuchi P, Sulzer M. Non-linear thermal networks – How can a meshed network improve energy efficiency? In: Proceedings of international conference CISBAT. Lausanne, Switzerland; 2015, p. 779–85.

[16] Gill B. Solving the large building all-electric heating problem. ASHRAE J 2021. URL https://tayloreng.egnyte.com/dl/hHl2ZkZRDC/ASHRAE_Journal_-_Solving_the_Large_Building_All-Electric_Heating_Problem.pdf_.

[17] Gabrielli P, Gazzani M, Martelli E, Mazzotti M. Optimal design of multi-energy systems with seasonal storage. Appl Energy 2018;219:408–24. http://dx.doi.org/10.1016/j.apenergy.2017.07.142, URL https://www.sciencedirect.com/science/article/pii/S0306261917310139.

[18] Gabrielli P, Acquilino A, Siri S, Bracco S, Sansavini G, Mazzotti M. Optimization of low-carbon multi-energy systems with seasonal geothermal energy storage: The anergy grid of ETH zürich. Energy Convers Manag: X 2020;8:100052. http://dx.doi.org/10.1016/j.ecmx.2020.100052.

[19] Kavanaugh S, Rafferty K. Geothermal heating and cooling – Design of ground-source heat pump systems. Atlanta, GA: ASHRAE; 2014, RP-1674.

[20] Mattsson SE, Elmqvist H. Modelica – An international effort to design the next generation modeling language. In: Boullart L, Loccufier M, Mattsson SE, editors. 7th IFAC symposium on computer aided control systems design. Gent, Belgium; 1997, p. 1–5.

[21] Crawley DB, Pedersen CO, Lawrie LK, Winkelmann FC. Energyplus: Energy simulation program. ASHRAE J 2000;42:49–56.

[22] Wetter M, Fuchs M, Grozman P, Helsen L, Jorissen F, Lauster M, et al. IEA EBC Annex 60 Modelica library – An international collaboration to develop a free open-source model library for buildings and community energy systems. In: The 14th international modelica conference, 2015. p. 395–402.

[23] Wetter M, van Treeck C, Helsen L, Maccarini A, Saelens D, Robinson D, et al. IBPSA Project 1: BIM/GIS and Modelica framework for building and community energy system design and operation – Ongoing developments, lessons learned and challenges. In: IOP conference series: earth and environmental science 323, 2019.

[24] Wetter M, Ehrlich P, Gautier A, Grahovac M, Haves P, Hu J, et al. OpenBuildingControl. Technical report, California Energy Commision; 2021, URL https://www.energy.ca.gov/sites/default/files/2021-05/CEC-500-2021-012.pdf.

[25] Wetter M, Zuo W, Thierry S, Nouidui T. Recent developments of the modelica buildings library for building energy and control systems. 2011, http://dx.doi.org/10.3384/ecp11063266.

[26] Wetter M, Benne K, Gautier A, Nouidui TS, Ramle A, Roth A, et al. Lifting the garage door on Spawn, an open-source BEM-controls engine. In: Proc. of building performance modeling conference and simbuild. Chicago, IL, USA; 2020, URL https://simulationresearch.lbl.gov/wetter/download/2020-simBuild-spawn.pdf.

[27] US Department of Energy. New construction – Commercial reference buildings – Version 1.4_7.2. 2012, https://www.energy.gov/eere/buildings/new-construction-commercial-reference-buildings.

[28] Bawaneh K, Nezami FG, Rasheduzzaman M, Deken B. Energy consumption analysis and characterization of healthcare facilities in the United States. Energies 2019;12. http://dx.doi.org/10.3390/en12193775.

[29] ANSI/ASHRAE 621-2019. Ventilation for acceptable indoor air quality. Standard, Atlanta, GA: ASHRAE; 2019.

[30] ASHRAE. Sequences of operation for common HVAC systems. Guideline, Atlanta, GA: ASHRAE; 2006.

[31] Wetter M, Ehrlich P, Gautier A, Grahovac M, Haves P, Hu J, et al. OpenBuildingControl: Digitizing the control delivery from building energy modeling to specification, implementation and formal verification. Energy 2022;238. http://dx.doi.org/10.1016/j.energy.2021.121501.

[32] ASHRAE. Fundamentals. Atlanta, GA: ASHRAE; 2017.

[33] Mathew P, Sanchez L, Lee SH, Walter T. Assessing the energy resilience of office buildings: Development and testing of a simplified metric for real estate stakeholders. Buildings 2021;11. http://dx.doi.org/10.3390/buildings11030096.

[34] Durkin TH, Rishel JB. Dedicated heat recovery. ASHRAE J 2003.

[35] Cline L, Bakkum B. Applications engineering manual – Central geothermal systems. TRANE; 2020, SYS-APM009C-EN.

[36] Taylor Engineering LLP, Taylor ST, Gill B, Kiriu R. Advanced sequences of operation for HVAC systems – Phase II Central plants and hydronic systems. Technical report research project 1711. Task 5: Reporting of findings, Atlanta, GA: ASHRAE; 2019.

[37] Carslaw H, Jaeger J. Conduction of heat in solids. Oxford: Claremore Press; 1947.

[38] ETH Zürich. Anergy grid campus Hönggerberg – A dynamic underground storage system. 2020, URL https://ethz.ch/content/dam/ethz/main/eth-zurich/nachhaltigkeit/Dokumente/Anergienetz/200129_Anergienetz_A4_6s_Einzel_EN_RZ.pdf.

[39] Jorissen F, Wetter M, Helsen L. Simulation speed analysis and improvements of modelica models for building energy simulation. In: The 11th international Modelica conference. Versailles, France; 2015, http://dx.doi.org/10.3384/ecp1511859.